Published in final edited form as:
Biochemistry. 2009 September 15; 48(36): 8624–8635. doi:10.1021/bi9007098.

Developing dual and specific inhibitors of dimethylarginine dimethylaminohydrolase-1 and nitric oxide synthase: Toward a targeted polypharmacology to control nitric oxide[†]

Yun Wang[‡], **Arthur F. Monzingo**[§,¶], **Shougang Hu**[‡,¶], **Tera H. Schaller**[‡], **Jon D. Robertus**[§,¶,*], and **Walter Fast**[‡,¶,*]

[‡] Division of Medicinal Chemistry, College of Pharmacy, The University of Texas, Austin, Texas 78712

[§] Department of Chemistry and Biochemistry, The University of Texas, Austin, Texas 78712

[¶] Texas Institute for Drug and Diagnostic Development, The University of Texas, Austin, Texas 78712

Abstract

Molecules that block nitric oxide's (NO) biosynthesis are of significant interest. For example, nitric oxide synthase (NOS) inhibitors have been suggested as anti-tumor therapeutics, as have inhibitors of dimethylarginine dimethylaminohydrolase (DDAH), an enzyme that catabolizes endogenous NOS inhibitors. Dual-targeted inhibitors hold promise as more effective reagents to block NO biosynthesis than single-targeted compounds. In this study, a small set of known NOS inhibitors are surveyed as inhibitors of recombinant human DDAH-1. From these, an alkylamidine scaffold is selected for homologation. Stepwise lengthening of one substituent converts an NOS-selective inhibitor into a dual-targeted NOS/DDAH-1 inhibitor and then into a DDAH-1 selective inhibitor, as seen in the inhibition constants of N^5-(1-iminoethyl)-, N^5-(1-iminopropyl)-, N^5-(1-iminopentyl)- and N^5-(1-iminohexyl)-L-ornithine for neuronal NOS (1.7, 3, 20, >1,900 μM, respectively) and DDAH-1 (990, 52, 7.5, 110 μM, respectively). A 1.9Å X-ray crystal structure of the N^5-(1-iminopropyl)-L-ornithine : DDAH-1 complex indicates covalent bond formation between the inhibitor's amidino carbon and the active-site Cys274, and solution studies show reversible competitive inhibition, consistent with a reversible covalent mode of DDAH inhibition by alkylamidine inhibitors. These represent a versatile scaffold for the development of a targeted polypharmacological approach to control NO biosynthesis.

Nitric oxide (NO)[1] is often described metaphorically as a double-edged sword. When produced at cytotoxic concentrations by immune cells, NO attacks tumor cells where it induces

[†]This work was supported in part by grants from the National Institutes of Health (GM69754 to WF and AI075509 to JDR), the American Cancer Society (RSG0506101GMC to WF), the Robert A. Welch Foundation (F-1572 to WF and F-1225 to JDR), a seed grant from the Texas Institute for Drug and Diagnostic Development (TI-3D: Welch Foundation Grant # H-F-0032) and by the College of Natural Sciences support to the Center for Structural Biology.

* To whom correspondence should be addressed. WF: College of Pharmacy, PHAR-MED CHEM, The University of Texas, 1 University Station C0850, Austin, TX 78712; phone, (512) 232-4000; fax, (512) 232-2606; WaltFast@mail.utexas.edu. JDR: Department of Chemistry and Biochemistry, University of Texas, Austin, TX 78712; phone, (512) 471-3175; fax, (512) 471-6135; jrobertus@cm.utexas.edu.

[1]The abbreviations used are: NO, nitric oxide; NOS, nitric oxide synthase; DDAH, dimethylarginine dimethylaminohydrolase; NMMA, N^{ω}-methyl-L-arginine; ADMA, asymmetric N^{ω}, N^{ω}- dimethyl-L-arginine; L-NIO, N^5-(1-iminoethyl)-L-ornithine; L-IPO, N^5-(1-iminopropyl)-L-ornithine; L-IBO, N^5-(1-iminoisobutyl)-L-ornithine; SMTC, *S*-methyl-L-thiocitrulline; DTNB, 5,5′-dithiobis-(2-nitrobenzoic acid); OPA, *o*-phthalaldehyde; SDS-PAGE, sodium dodecyl sulfate polyacrylamide gel electrophoresis; ESI-MS, electrospray ionization mass spectrometry; NMR, nuclear magnetic resonance; PCR, polymerase chain reaction; HPLC, high performance liquid chromatography.

apopotosis and inhibits their growth and metastasis (2-4). However, when produced by tumor cells at lower concentrations (estimated to be at least 1-2 orders of magnitude lower than cytotoxic concentrations (5)) NO cuts the other way by *facilitating* tumor growth (4,6). For example, introduction of nitric oxide synthase into a human colonic adenocarcinoma cell line leads to increased growth and vascularity of implanted tumors (5). Significant low-level NO production has been found in malignant human breast, neuronal, gastric, cervical and ovarian cancers, but not in the surrounding benign tissues (6). In neuronal, breast, gynecological, head and neck tumors, NO levels have been shown to positively correlate with increasing tumor grade (5,6). Although the detailed mechanism of NO participation in tumor biology is still being elucidated, there is increasing evidence that its biosynthesis plays an important role in angiogenesis and tumor progression; thus inhibitors of NO production have been suggested as possible antitumor therapeutics (6,7).

In humans, NO is biosynthesized by nitric oxide synthase (NOS) from L-arginine (**1**), oxygen and NADPH in a highly regulated manner (Figure 1) (8). Natural regulation mechanisms can suggest useful targets for new therapeutics. One such regulation mechanism involves pools of endogenously produced NOS inhibitors, N^{ω}-methyl-L-arginine (NMMA, **2**) and asymmetric N^{ω}, N^{ω}-dimethyl-L-arginine (ADMA, **3**) (9-12). The concentrations of these methylated arginines are controlled in turn by another enzyme, dimethylarginine dimethylaminohydrolase (DDAH), which hydrolyzes both substrates to yield L-citrulline (**4**) and the corresponding alkylamine, thus relieving the inhibition of NOS and promoting NO biosynthesis (Figure 1) (13,14). Notably, DDAH activity has been detected in a series of human tumors and is particularly high in brain tumors (15). Artificial over-expression of DDAH in a glioma cell line leads to increased NO synthesis, increased production of vascular endothelial cell growth factor and increased angiogenesis (16). Tumors derived from these cells grow almost twice as fast as controls, highlighting the importance of DDAH to tumor progression (16). Therefore, inhibitors of both NOS and DDAH may serve as antitumor therapeutics.

Designing such inhibitors presents a challenge. NOS and DDAH have similar yet distinct specificities; they share the same product, yet substrates of each enzyme can inhibit the other. There are also multiple isoforms of both enzymes, each with distinct tissue distributions. Selective inhibitors could be very useful as therapeutic agents - considerable progress has recently been made designing isoform-selective NOS inhibitors (17-19). However, single compounds capable of inhibiting both NOS and DDAH are also desirable because both of these enzymes promote NO production. Such dual-targeted inhibitors could potentially achieve more effective inhibition of biological NO production than single-target agents. Therefore, understanding the similarities and differences between these enzymes' pharmacophores is of considerable interest for developing specific pharmacological tools and dual-targeted drugs.

Toward these ends, a small set of known NOS inhibitors are tested for their ability to inhibit recombinant human DDAH-1. The most potent are alkylamidines and this scaffold is selected for homologation. Simple alterations in chain length result in dual-targeted inhibitors or compounds selective for inhibition of either DDAH-1 or NOS. The mechanism of DDAH-1 inhibition by one of the dual-targeted inhibitors is characterized in detail and the implications for design of a targeted polypharmacology for NO control are discussed.

Materials and Methods

Materials

Synthetic DNA primers were from Invitrogen (Carlsbad, CA). Chelex-100 was purchased from Bio-Rad (Hercules, CA). Aminoguandine hemisulfate, 1-amino-2-hydroxyguanidine, 2-ethyl-2-thiopseudourea and N^5-(1-imnioethyl)-L-ornithine (L-NIO) were purchased from Calbiochem (San Diego, CA), *N*-(3-(Aminomethyl)benzyl) acetamidine (1400W) and

phenylene-1, 3-bis(ethane-2-isothiourea) from Alexis Biochemicals (San Diego, CA), *S*-Ethyl-*N*-phenylisothiourea from Toronto Research Chemicals (North York, Canada) and N^{α}-*t*-butyloxycarbonyl (BOC)-L-ornithine from Bachem (Torrance, CA). Unless specified otherwise, all other chemicals were from the Sigma Aldrich Chemical Co. (St Louis, MO). Figures depicting bond-line notations of chemical structures were prepared using ChemDraw (CambridgeSoft, Cambridge, MA). Figures depicting protein structures were prepared using UCSF Chimera (20) or Pymol (DeLano Scientific, Palo Alto, CA).

General procedure for synthesis of N^5-(1-iminoalkyl)-L-ornithines

Proprionitrile, isobutyronitrile, pentanenitrile and hexanenitrile were each converted into their corresponding ethyl imidic esters and then to N^5-(1-iminoalkyl)-L-ornithines by a general procedure similar to syntheses reported elsewhere (21-24). The starting nitrile (10-100 mmol) was mixed with anhydrous ethanol (2.6 equiv), cooled to 0° C and bubbled through with dry $HCl_{(g)}$ for 1 h. The resulting solution was then stirred for an additional 4 h at 0° C and then overnight at room temperature. The reaction mixture was purged with $N_{2(g)}$ to remove most of the dissolved HCl, and volatile solvents were removed by reduced pressure rotary evaporation. The resulting residue was washed with cold diethylether and dried to afford the imidate as a white solid or foam. The imidate (2 - 3 equiv) was slowly added in portions to a solution of N^{α}-BOC-L-ornithine (1 mmol) in water (5 mL) at 5° C while keeping the reaction pH near 10 by dropwise addition of NaOH (2.5 M). After stirring for 1.5 h, the reaction pH was adjusted to 7 using HCl (1 M). The resulting mixture was stirred overnight and loaded onto Dowex 50WX8-400 ion exchange resin, washed with water, and eluted with 10% aqueous pyridine. After removal of volatile solvents by reduced pressure rotary evaporation, the resulting solid was treated with HCl (6 M) in ethyl acetate (10 mL) at 0° C for 1.5 h and allowed to warm to room temperature for 2 h. After removal of volatile solvents by reduced pressure rotary evaporation, the N^5-(1-iminoalkyl)-L-ornithine is afforded as a white or off-white foam with typical yields from 84 – 94 % from the N^{α}-BOC-L-ornithine starting material.

N^5-(1-iminopropyl)-L-ornithine

^{1}H-NMR (300 MHz, D_2O) δ: 3.99 (1H, t, J = 6.0 Hz), 3.20 (2H, t, J = 6.9Hz), 2.35 (2H, t, J = 7.8Hz), 1.92-1.57 (4H, m), 1.09 (3H, t, J = 7.5Hz). ^{13}C-NMR (D_2O): 171.86, 169.61, 52.67, 41.40, 27.20, 26.63, 22.89, 10.88. HRMS-ESI(m/z): $M+H^+$ calcd for $C_8H_{18}N_3O_2$, 188.1394, found 188.1394.

N^5-(1-iminoisobutyl)-L-ornithine

^{1}H-NMR(300 MHz, D_2O) *δ*: 3.93 (1H, t, *J* = 6.3 Hz), 3.20 (2H, t, *J* = 6.6 Hz), 2.63 (1H, m, *J* = 6.9 Hz), 1.85 (2H, m), 1.65 (2H, m), 1.11 (6H, d, *J* = 6.9 Hz). ^{13}C-NMR (D_2O): 172.84, 171.88, 52.64, 41.23, 33.23, 27.15, 22.80, 19.01. HRMS (ESI) (m/z): $M+H^+$ calcd for $C_9H_{20}N_3O_2$, 202.1550, found 202.1551.

N^5-(1-iminopentyl)-L-ornithine

^{1}H-NMR (300 MHz, D_2O) *δ*: 3.94 (1H, t, *J* = 5.4 Hz), 3.19 (2H, t, *J* = 6.9 Hz), 2.33 (2H, t, *J* = 7.8 Hz), 1.92-1.56 (4H, m), 1.56-1.44 (2H, m), 1.28-1.14 (2H, m), 0.76 (3H, t, *J* = 7.2 Hz). ^{13}C-NMR(D_2O): 171.91, 168.61, 52.69, 41.31, 32.64, 28.77, 27.20, 22.84, 21.36, 12.97. HRMS-ESI(m/z): $M+H^+$ calcd for $C_{10}H_{22}N_3O_2$, 216.1712, found 216.1709.

N^5-(1-iminohexyl)-L-ornithine

^{1}H-NMR(300MHz, D_2O) *δ*: 3.89 (1H, t, *J* = 6.0 Hz), 3.20 (2H, t, *J* = 6.9 Hz), 2.33 (2H, t, *J* = 7.5 Hz), 1.90-1.80 (2H, m), 1.70-1.40 (4H, m), 1.24-1.10 (4H, m), 0.73 (3H, t, *J* = 6.9 Hz). ^{13}C-NMR (D_2O): 172.32, 168.68, 52.99, 41.40, 32.91, 30.23, 27.35, 26.37, 22.92, 21.71, 13.29. HRMS-ESI(m/z): $M+H^+$ calcd for $C_{11}H_{24}N_3O_2$, 230.1863, found 230.1864.

Cloning of recombinant human DDAH-1

Heterologous overexpression of human DDAH-1 using the pET28a-*h*DDAH-1 plasmid (25) produces a fraction of total protein that is *N*-terminal gluconoylated (26), as is also seen with other proteins overexpressed using similar vectors (27). This modification could introduce unwanted complexity to electrospray ionization mass spectrometry (ESI-MS) analysis. To avoid gluconoylation, the *N*-terminus was re-engineered by introducing the mutations suggested by Geoghegan et al (27), changing the encoded sequence from $MGSSH_6$- to MPH_6- in two experimental steps. First, the encoded $MGSSH_6$- sequence was mutated to encode MAH_6- by using specific end primers: 5′-AATCCATGGCGCATCATCATCATCATCACAG-3′ and 5′-TCTTGGATCCTCAGGAGTCTACTTTCTTG-3′. The forward primer contains an *Nco*I restriction site (underlined) followed by 22 bases, which encode the mutated *N*-terminal sequence. The reverse primer contains a *Bam*HI restriction site (underlined) followed by 19 bases complementary to a stop codon and the codons for the *C*-terminal DDAH-1 sequence. PCR amplification was carried out using an MJ Research (Waltham, MA) PTC 200 thermal cycler. Reactions included the primers described above, the pET28a-*h*DDAH-1 template, dNTPs, and *pfu* polymerase in the *pfu* polymerase buffer (Stratagene, La Jolla, CA) as described in the manufacturer's instructions, with a temperature program of 95° C for 2 min, followed by 2 cycles of 95° C for 30 s, 44° C for 30 s and 72° C for 1 min, followed by 26 cycles of 95° C for 30 s, 54° C for 30 s and 72° C for 1 min, followed by 10 min at 72° C for polishing. The PCR-amplified product and the expression vector pET-28a (EMD Biosciences, San Diego, CA) were digested with *Nco*I and *Bam*HI restriction enzymes (New England Biolabs, MA) and the small fragments removed by Qiaquick purification (Qiagen, Valencia, CA) before ligation. The resulting intermediate plasmid was subjected to a second step in which the sequence encoding MAH_6- was changed to MPH_6- by Quickchange site-directed mutagenesis (Stratagene), using the mutagenic oligonucleotides 5′-CTTTAAGAAGGAGATATACCATGCCGCATCATCATCATCATCAC-3′ and 5′-GTGATGATGATGATGATGCGGCATGGTATATCTCCTTCTTAAAG-3′ (mutations underlined). A PCR mixture containing the intermediary plasmid generated above as a template, the mutagenic primers, a dNTP mixture and *pfuTurbo* DNA polymerase in the manufacturer's buffer (Stratagene) was run using a temperature program of 95° C for 30 s, followed by 12 cycles of 95° C for 30s, 55° C for 1 min, and 68° C for 13 min. *Dpn*I was then added to the cooled reaction mixture to digest the methylated parent plasmid. After incubation at 37° C for 1 h, the mixture was transformed into DH5α *E. coli* cells and selected on LB agar plates supplemented with kanamycin (30 μg/mL). The final plasmid, pET28a-hDDAH-1re, was purified from an overnight culture and the gene insert was fully sequenced (DNA Facility, University of Texas at Austin) to verify the desired sequence.

Site-directed mutagenesis to generate L30A, E78A and L271G mutations

Three site-directed mutations of DDAH-1 were constructed using a QuikChange site-directed mutagenesis kit (Stratagene). Briefly, three pairs of oligonucleotides: 5′-CCAGCACGCGGCGAGAAGCGCC-3′ and 5′ GGCGCTTCTCGCCGCGTGCTGG-3′; 5′-CGTCTTCGTGGCGGACGTGGCCGTGGTGTGC-3′ and 5′-GCACACCACGGCCACGTCCGCCACGAAGACG-3′; 5′-GGTGGATGGGGGGCTCACCTGCTGC-3′ and 5′-GCAGCAGGTGAGCCCCCCATCCACC-3′ were used to introduce the L30A, E78A and L271G mutations (underlined), respectively. Each PCR mixture contained template plasmid (pET28a-hDDAH-1re), one pair of mutagenic primers, a dNTP mixture and *pfuTurbo* DNA polymerase in the manufacturer's buffer (Stratagene). Reactions were subjected to a temperature program of 95° C for 30 s, followed by 16 cycles of 95° C for 30 s, 55° C for 1 min, and 68° C for 13 min. After cooling, *Dpn*I was added digest the methylated parent plasmid and the remaining mixture was transformed into DH5α *E. coli* cells and selected for resistance

on LB agar plates supplemented with kanamycin (30 μg/mL). The resulting plasmids (pET28a-hDDAH-1re-L30A, -E78A and –L271G) were purified from overnight cultures and the inserts fully sequenced to verify the correct sequences.

Expression and Purification of DDAH-1

Recombinant DDAH-1 was overexpressed in BL21 (DE3) *E. coli* using pET28a-hDDAH-1, pET28a-hDDAH-1re or one of the three expression vectors encoding a mutant DDAH-1 (described above), using the same procedure described earlier (1), except that 30 μg/mL kanamycin was used. The resulting frozen cell pellets were resuspended in a total of 60 mL His-tag Lysis Buffer (50 mM NaH_2PO_4, 300 mM NaCl, 10 mM imidazole, 15% glycerol, pH 8.0) and sonicated on ice for 5 min with 15 s pulses at 30 s intervals using a sonic dismembrator (Fisher Scientific Model 500, large tip). Cell debris was pelleted twice by centrifugation at 34,957 × g for 15 min. The resulting supernatant was incubated batchwise with Lysis Buffer-equilibrated Ni-NTA affinity resin (8 mL, Qiagen) for 1 h. The resin was subsequently packed into a column (2 cm diameter), washed with Lysis Buffer (40 mL) and Wash Buffer (50 mL, 50 mM NaH_2PO_4, 300 mM NaCl, 20 mM imidazole, 15% glycerol, pH 8.0) and the desired protein removed with Elute Buffer (15 mL, 50 mM NaH_2PO_4, 300 mM NaCl, 250 mM imidazole, 15% glycerol, pH 8.0). Fractions containing DDAH-1 as gauged by SDS-PAGE (migrating at approximately 33 kDa), were pooled and concentrated using Amicon Ultra Centrifugal Filter devices (Millipore, Billerica, MA) with a 10 kDa molecular weight cutoff (MWCO). The concentrated protein fractions (approx 300 μL) were diluted in 20 mL Buffer A (50 mM KH_2PO_4, 3.0 M NaCl, 2 mM 1,10-phenanathroline, 3 mM dithiothreitol, 15% glycerol, pH 7.0) and loaded onto a 1.5 × 18 cm phenyl-Sepharose column (GE Healthcare, Piscataway, NJ). Proteins were eluted using a linear gradient from 100% Buffer A to 100% Buffer B (50 mM KH_2PO_4, 2 mM 1,10-phenanathroline, 3 mM dithiothreitol, 15% glycerol, pH 7.0). As gauged by SDS-PAGE, fractions containing DDAH-1 were pooled and concentrated to approximately 1 mL using an Amicon Ultra Centrifugal Filter (10 kDa MWCO). The final protein was dialyzed for 4 × 5 h against 500 mL aliquots of Chelex 100-treated (BioRad) Dialysis Buffer (50 mM KH_2PO_4, 10% glycerol, pH 7.0), flash frozen and stored in aliquots at -80° C. All of the DDAH-1 variants purified using this method were homogenous by coomassie-stained SDS-PAGE. Wild-type, the *N*-terminal variant, and the L30A, E78A and L271G variants of DDAH-1 were all purified using the same procedure, with typical yields of 1-2 mg / L culture.

Each purified protein was analyzed by ESI-MS (Analytical Core Facility, College of Pharmacy, The University of Texas) and gave their expected masses (all in Da): Wild-type from pET-28a-hDDAH-1:MW_{calc} = 33,441, MW_{exptl} = 33,434 (major), 33,612 (minor); *N*-terminal variant from pET-28a-hDDAH-1re: MW_{calc} = 33,311, MW_{exptl} = 33,304 (Reconstruction of the *N*-terminus successfully removed the minor +177 Da gluconylation peak); L30A: MW_{calc} = 33,269, MW_{exptl} = 33,263; E78A: MW_{calc} = 33,253, MW_{exptl} = 33,247; L271G: MW_{calc} = 33,245, MW_{exptl} = 33,247.

To determine metal content, purified protein samples (approximately 120 μM) and buffer-only controls were analyzed by inductively coupled plasma mass spectrometry (Department of Geological Sciences of The University of Texas at Austin). Metal ion binding was calculated by subtracting the concentration of metal ions found in the buffer from those found in the protein sample and dividing by the protein concentration. Protein concentrations were determined by measuring the absorption at 280 nm in buffer containing 6 M guanidinium hydrochloride and 20 mM phosphate (pH 6.5). The extinction coefficient of the protein (7,680 M^{-1} cm^{-1}) was calculated on the basis of the amino acid sequence (http://workbench.sdsc.edu/) (28). Although protein preparations that omit 1,10-

phenanthroline harbor approximately 0.4 equivalents of inhibitory Zn(II), the procedure above yields DDAH-1 and variants that contain only trace amounts of Zn(II).

Steady-State Kinetic Studies

To determine the steady-state kinetic constants for hydrolysis of N^{ω},N^{ω} –dimethyl-L-arginine (ADMA, **3**), a discontinuous colorimetric assay based on diacetylmonoxime derivatization of L-citrulline (**4**) was used, as described previously (29). To measure the steady-state kinetic constants for hydrolysis of *S*-methyl-L-thiocitrulline (SMTC, **5**), a continuous spectrophotometric assay based on 5,5′-dithiobis(2-nitrobenzoic acid) (DTNB) derivatization of the methanethiol product was used, as described previously for DDAH from *Pseudomonas aeruginosa* (30). Recombinant human DDAH-1 showed linear kinetics for > 10 min, despite the presence of six cysteine residues in its sequence, indicating that DDAH-1 is not inhibited by DTNB over this timescale. To obtain steady-state constants, KaleidaGraph software (Synergy Software, Reading, PA) was used to directly fit observed rates at various substrate concentrations to the Michaelis-Menten equation. The constants obtained for hydrolysis of SMTC are somewhat different from those reported earlier (1), likely due to the ability of the continuous assay to more precisely define the linear phase of the hydrolysis kinetics.

Survey of selected NOS inhibitors as DDAH inhibitors

A small set of commercially available NOS inhibitors, 2-ethyl-2-thiopseudourea (**6**), *S*-ethyl-*N*-phenylisothiourea (**7**), phenylene-1,3-bis(ethane-2-isothiourea) (**8**), aminoguanidine (**9**), 1-amino-2-hydroxyguanidine (**10**), *N*-(3-(aminomethyl)benzyl)acetamidine (**11**) and N^5-(1-imnioethyl)-L-ornithine (**12**), were each dissolved in assay buffer (100 mM KH_2PO_4, 1 mM EDTA, pH 7.27) to final concentrations between 0 – 1 mM, with each mixture also containing the substrate *S*-methyl-L-thiocitrulline (SMTC, **5**). Although the K_M of SMTC is 3 μM, inhibitor screens were carried out at 25 μM of SMTC to insure linearity throughout the experimental timescale (approximately 5 min). Upon addition of DDAH-1 (1 μM), hydrolysis kinetics were measured using the continuous assay described above. IC_{50} constants were determined by fitting observed reaction rates at over a series of inhibitor concentrations to equation 1, and corresponding K_i values were calculated from the IC_{50} values using equation 2, assuming competitive inhibition (31, 32):

$$\%\text{Activity} = \frac{100}{1 + \frac{[\text{Inhibitor}]}{IC_{50}}} \quad (1)$$

$$K_i = \frac{IC_{50}}{1 + [\text{SMTC}]/K_M} \quad (2)$$

Turnover and Time-dependent Inhibition Experiments

The three *S*-alkylisothiourea compounds tested as inhibitors were also assayed as potential DDAH-1 substrates by using the continuous assay described above, but omitting SMTC from the assay mixture. L-IPO (**13**) was assayed as a DDAH-1 substrate by preparing 18 h incubation mixtures (at 25°C) of L-IPO (6 mM) in assay buffer with and without DDAH-1 (10 μM). The reaction mixtures were diluted 3-fold and subjected to Amicon Ultra Centrifugal Filter devices (10 kDa MWCO) to remove protein. These reaction mixtures were then derivatized using the fluorogenic reagent *o*-phthalaldehyde (OPA, Agilent Technologies, Santa Clara, CA), which reacts selectively with primary amines. The OPA regent (10 μL) was mixed with an equal

volume of reaction mixtures and incubated for 1 min in the dark. The resulting mixture was then separated by a Shimadzu Prominence high performance liquid chromatograph (HPLC) (Columbia, MD) using a Agilent Eclipse XDB-C18 column (4.6 mm × 250 mm, 5 μm particle size) and a linear gradient from 8.7 % - 70 % Buffer B (Buffer A: 30 mM Na_3PO_4 pH 7.56, Buffer B: 100% acetonitrile) and fluorescent detection of the derivatized products (ex: 340 nm; em: 455 nm).

Preincubation mixtures were used to test whether L-IPO (**13**) displays time dependent inhibition of DDAH-1. Briefly, L-IPO (10 mM) was mixed with hDDAH-1 (80 μM) and incubated 18 hr at 25°C. L-Citrulline (**4**) (66.7 mM) and no inhibitor were used in control experiments done in parallel. Before and after incubation, aliquots (6 μL) of the reaction mixtures were rapidly diluted approx 40-fold into the continuous assay buffer containing the substrate SMTC (25 μM) to monitor initial hydrolysis rates.

Reversible Inhibition by IPO

Varying concentration of L-IPO (**13**) (0-500 μM) and SMTC (**5**) (2-256 μM) were mixed in Assay buffer and monitored using the continuous kinetic assay. To obtain a numerical value for K_i, the initial rate data were fit directly using a competitive inhibition model (Equation 3) to determine α values, and a linear fit of these α to Equation 4. For easy visual interpretation, the same data are also presented graphically as a double reciprocal Lineweaver-Burke plot. K_i values for L-IPO (**13**) inhibition of mutant DDAH-1 preparations were calculated from IC_{50} values, determined as described above.

$$v_o = \frac{V_{\max}\,[S]}{\alpha K_M + [S]} \tag{3}$$

$$\alpha = 1 + \frac{[I]}{K_i} \tag{4}$$

Analytical Sedimentation Equilibrium Ultracentrifugation

Triplicate experiments using 2-channel centerpieces were carried out using a Beckman Optima XL-I analytical ultracentrifuge with the rotor speed set to 20,000 rpm at 25.0 °C. Ultracentrifuge cells contained DDAH-1 (1 mg / mL) in Chelex 100-treated buffer (20 mM NaH_2PO_4 and 100 mM NaCl, pH 7.0), the same conditions as reported for characterization of the DDAH from *Pseudomonas aeruginosa* (33). Thirteen absorbance scans at 240 nm were performed for each cell, the first after 10 min, and the remaining scans after an additional 2, 4, 8, 16, 26, 29, 31, 33, 35, 37, 39, 41, 43 and 45 h. Absorbance data were extracted and fitted using Ultrascan II version 8.0 software (34). A partial specific volume ($\bar{v}$) of 0.7390 mL / g (predicted by Sednterp 1.07 software, www.bbri.org/RASMB/rasmb.html) and a buffer density (ρ) of 1.0 g / mL were used in the analysis. The data were fitted globally to a one component ideal species model using equation 5, where X = radius, Xr = reference radius, A = amplitude of monomer*, M = molecular weight of monomer*, E = extinction coefficient, R = gas constant, T = temperature, B = baseline*, ω = angular velocity (* indicates this parameter was floated) (34).

$$C(X) = e^{\left[\frac{\ln(A) + M\omega^2(1-\bar{v}\rho)(X^2 - X_r^2)}{2RT}\right]} + B \tag{5}$$

Crystallization and Data Collection

The human DDAH-1 was concentrated to approximately 13 mg / mL in 50 mM potassium phosphate, pH 7.0, 10% glycerol using an Amicon Ultra Centrifugal Filter (10 kDa MWCO). The protein was crystallized at 4° C using the hanging drop method from 25% (w/v) PEG6000, 0.1 M Tris-HCl, pH 8.0. For the purpose of determining the structure of DDAH-1 in complex with N^5-(1-iminopropyl)-L-ornithine (L-IPO), a crystal was transferred to a reservoir containing 20 μL 5 mM L-IPO in artificial mother liquor (25% PEG 6000, 0.1 M Tris-HCl, pH 8.0) and soaked overnight. Prior to data collection, crystals were treated with cryoprotectant by transferring to 30% PEG6000, 0,1 M Tris-HCl, pH 8.0 for 1-5 seconds. Crystals mounted in a cryoloop (Hampton Research, Laguna Niguel, CA), were frozen by dipping in liquid nitrogen and placed in the cold stream on the goniostat.

X-ray diffraction data were collected from the apo-DDAH-1 crystal at 100° K on an RAXIS IV++ image plate detector (Rigaku, The Woodlands, TX) with X-rays generated by a Rigaku RU-H3R rotating anode generator operated at 50 mV, 100 mA. Diffraction data from the inhibitor soaked crystals were collected at the X-ray Crystallography Core Laboratory at the University of Texas Health Science Center at San Antonio. Data were collected at 100° K on a R-AXIS HTC image plate detector with X-rays generated by a Rigaku MicroMax-007HF rotating anode generator operated at 40 mV, 30 mA. Diffraction images were processed and data reduced using HKL2000 (35).

Structure Determination and Analysis

The structure of the apo-human DDAH-1 was solved by molecular replacement with MOLREP (36) and the Evolutionary Protein Molecular Replacement (EPMR) program (37) using the structure of human DDAH-1 complexed with citrulline (PDB accession code 2JAI) (38), with citrulline omitted, as the search model. The structure of human DDAH-1 complexed with L-IPO was solved by molecular replacement with Phaser (39) using the structure of human DDAH-1 as the search model.

Model building was carried out using O (40). Refinement of models was performed with the Crystallography and NMR System (CNS) (Version 1.1) (41) using the slow-cooling protocol. Analysis of the diffraction data from the L-IPO complex crystal using Phenix indicated the presence of pseudo-merohedral twinning. Refinement of the complex data, accounting for the crystal twinning, was done with Phenix (42). There were several rounds of refinement followed by manual rebuilding of the model. To facilitate manual rebuilding, a difference map and a $2F_0$-F_c map, σ_A-weighted to eliminate bias from the model (43), were prepared. 5% of the diffraction data were set aside throughout refinement for cross-validation (44). PROCHECK (45) and MolProbity (46) were used to determine areas of poor geometry and to make Ramachandran plots. Computations and model building were carried out on an HP Pavilion a1610n (Hewlett-Packard Co., Palo Alto, CA) computer.

Atomic coordinates

Coordinates of the refined model of the apo-human DDAH-1 and the human DDAH-1 complexed with L-IPO have been deposited in the Protein Data Bank with entry codes 3I2E and 3I4A, respectively.

Results and Discussion

Survey of selected NOS inhibitors as DDAH-1 inhibitors

As a limited exploration of the chemical space shared by ligands of both NOS and DDAH, a small set of known NOS inhibitors was assayed for inhibition of recombinant human DDAH-1. The results are included, along with related compounds, in a graphical summary (Figure 2).

To simplify the discussion, only the K_i values for nNOS are listed (Table 1) because these compounds do not show significant selectivity between the three isoforms of NOS, and nNOS co-localizes to many of the same tissues as DDAH-1 (47).

Three *S*-alkyl isothiourea compounds, *S*-ethyl-2-thiopseudourea (**6**), *S*-ethyl-*N*-phenylisothiourea (**7**) and phenylene-1,3-bis(ethane-2-isothiourea) (**8**) (nNOS K_i = 29, 120 and 250 nM, respectively) (48,49) do not inhibit DDAH-1 at concentrations ≤ 1 mM. These compounds were also tested as substrates of DDAH-1 because the structurally related *S*-methyl-L-thiocitrulline (SMTC, **5**) is a good DDAH substrate (DDAH-1: k_{cat} = 2.5 min^{-1}; K_M = 3 μM) as well as a known nNOS inhibitor (K_i = 50 nM) (50). None of these three compounds were processed as DDAH-1 substrates during 15 min incubations. Therefore, structural elaboration of the thiourea scaffold was not pursued further. Aminoguanidines were the second type of inhibitory fragment surveyed. Both aminoguanidine (**9**) and 1-amino-2-hydroxyguanidine (**10**) (nNOS K_I = 55 and 680 μM, respectively) (51,52) do not serve as effective inhibitors of DDAH-1, and so were not studied further. The third structural class tested as DDAH-1 inhibitors are amidines: *N*-(3-aminomethyl)benzylacetamidine (1400W, **11**) and N^5-(1-iminoethyl)-L-ornithine (L-NIO, **12**) (nNOS K_i = 2 and 1.7 μM, respectively) (24,53). Compound 1400W (**11**) does not inhibit DDAH-1 at concentrations ≤ 1 mM, but L-NIO (**12**) does inhibit weakly (K_i = 990 μM), suggesting that the amidino group may be a promising scaffold on which to construct a dual-targeted inhibitor. It is likely that the alpha amino group and carboxylate of **12** play a significant role in binding to both enzymes, but their contribution was not quantified here. Rather, an expanded set of alkyl substituted amidines was prepared and tested.

Survey of selected amidino-based NOS inhibitors as DDAH-1 inhibitors

A series of alkyl-substituted amidines have previously been reported as NOS inhibitors (23, 24,54). Notably, compounds with shorter alkyl substituents - (N^5-(1-iminoethyl)- through N^5-(1-iminopentyl)-L-ornithine (**12-14**) - are potent NOS inhibitors, but the slightly longer homolog N^5-(1-iminohexyl)-L-ornithine (**15**), can not effectively inhibit NOS.

We synthesized and tested a similar set of several alkyl-substituted amidines as potential inhibitors of DDAH-1: N^5-(1-iminoethyl)-L-ornithne (L-NIO, **12**), N^5-(1-iminopropyl)-L-ornithine (L-IPO, **13**), N^5-(1-iminopentyl)-L-ornithine (**14**), and N^5-(1-iminohexyl)-L-ornithine (**15**). All of these compounds inhibit DDAH-1 with micromolar K_i values (8 to 990 μM, Table 2). Extending the alkyl substituent of **12** by one methylene group to form L-IPO (**13**) translates into a 20-fold increase in potency. Further extension of the alkyl chain by an additional two methylene units to form **14**, translates to a further 7-fold increase in potency. Branching the alkyl chain does not greatly increase potency; N^5-(1-iminoisobutyl)-L-ornithine (L-IBO, structure not shown) has a K_i value that matches (within error) that of L-IPO (**13**). Linear chain extension to **15** decreases the affinity for DDAH-1 somewhat, but inhibition is still evident (K_i = 110 μM). These results contrast sharply with the same compounds' potency for inhibiting nNOS. In particular, extending the chain length from that of L-IPO (**13**) to the longest amidine tested here, **15**, results in a 2-fold decrease in potency for DDAH-1 inhibition, but a > 1000-fold decrease in potency for nNOS inhibition (54). It is interesting to note that two previously reported DDAH-selective inhibitors, N^{ω}-(2-methoxyethyl)-L-arginine (L-257, **16**) (38,55) and N^{ω}-(but-3-enyl)-L-arginine (**17**) (56) are approximately the same length as **15**, suggesting that these compounds may achieve their specificity for DDAH through similar means. However, there are probably alternative methods to achieve selectivity, because the shorter analog *S*-2-amino-4-(3-methylguanidino)butanoic acid (4124W, **18**) is also selective for DDAH, albeit with weak potency (IC_{50} = 1.5 mM for a crude rat kidney DDAH preparation) (11,55). Further modifications of the alkyl chain may also increase potency or selectivity; Kotthaus et al recently reported a series of alkenyl-amidines capable of dual inhibition, of which N^5-(1-imino-3-

butenyl)-L-ornithine (**19**) is the most potent ($K_{i,\ DDAH\text{-}1}$ = 2 μM; $K_{I,\ nNOS}$ = 90 nM) (24,56). One of the dual-targeted inhibitors, L-IPO (**13**) was selected for more detailed studies (below).

Analytical Equilibrium Sedimentation Ultracentrifugation

Both monomeric and dimeric DDAH isoforms have been reported (33,57), and the closely related enzyme arginine deiminase has shown half-sites reactivity (58). Therefore, to establish the minimal catalytic unit of human DDAH-1, the oligomeric state of its apo form in solution was determined by analytical equilibrium sedimentation ultracentrifugation at 1mg / mL, pH 7.0, 20° C. Each set of experimental data that had reached equilibrium was collected and subjected to a global simultaneous fit to a single ideal species model (Figure 3). The fitted molecular weight (34,530 Da) matched well with the theoretical monomer molecular weight (33,558 Da); variance = $8.7e^{-5}$. Therefore, human DDAH-1 is assigned as a monomeric enzyme.

X-ray Crystallography

Human DDAH-1 crystallized in space group $P2_1$, with cell constants a = 73.0, b = 47.9, c = 90.3 Å, β = 94.1°, and with two molecules per asymmetric unit, giving a V_m of 2.5 Å / dalton. The structure was solved by molecular replacement using the structure of human DDAH-1, previously reported in complex with citrulline (PDB accession code 2JAI) (38), as the search model. The final 2.0 Å structure consists of residues 8-282; residues 1-7 and 283-285 are not visible in electron density maps and are presumed to be disordered.[2] Crystallographic data are shown in Table 3. The two DDAH-1 molecules in the asymmetric unit are virtually identical with an rms distance between equivalent Cα positions of 0.16 Å. Similarly, the rmsd between Cαs of the apo-DDAH-1 and the previously reported complexed DDAH-1 (38) is 0.45 Å. The largest difference between the two apo-DDAH-1 molecules in the asymmetric unit is found in a loop (residues 168-171) adjacent to the active site. This loop was found disordered in the DDAH-1/citrulline complex structure.

The crystal of DDAH-1 in complex with L-IPO was also found to be of space group $P2_1$, but with cell constants a = 47.6, b = 80.1, c = 73.9 Å, β = 90.1°, and with two molecules per asymmetric unit, giving a V_m of 2.4 $Å^3$ / dalton. The structure was solved by molecular replacement using the structure of apo-DDAH-1 as the search model. The final 1.9 Å structure consists of residues 5-282; residues 1-4 and 283-285 are not visible in electron density maps and are presumed to be disordered. The bound DDAH-1 is very similar to the apo-enzyme with an rms distance between equivalent Cα positions of 0.30 Å. Several crystal forms of DDAH-1 have been obtained from the crystallization conditions used.

The overall structure determined for human DDAH-1 in complex with L-IPO (**13**) is very similar to those described earlier for human DDAH-1 in complex with L-citrulline and with the inhibitor N^{ω}-(2-methoxyethyl)-L-arginine (L-257, **16**) (38). However, inspection of the electron density maps near the active site reveals some unexpected features (Figure 4). Continuous density is observed between the active-site Cys274 side chain and the bound inhibitor. The remaining interactions with the bound inhibitor and the enzyme are quite similar to those reported for other inhibitors and those proposed for DDAH substrates (38,59,60). The continuous density between enzyme and inhibitor suggests that the active site Cys274 side chain can attack the amidino carbon (C^{ζ}), resulting in a tetrahedral complex (**21**) (Figure 5). This structure is reminiscent of the related structure of an sp^2 hybridized thiouronium reaction intermediate trapped in a mutant DDAH from *P. aeruginosa* (60), but the density observed here at the active site of human DDAH-1 can better accommodate a tetrahedral sp^3 species.

[2]The amino acid numbering is based on that described in (1). For example, the active site Cys nucleophile is assigned as residue 274.

Characterization of DDAH-1 inhibition by L-IPO (13)

As a complement to structural studies, the inhibition of DDAH-1 by L-IPO (**13**) was studied in more detail. Lineweaver-Burke plots of $1/v_o$ and 1/[S] at varying concentrations of L-IPO (**13**) show intersecting lines at the y-axis, consistent with substrate and inhibitor competing for binding to the same site on DDAH-1 (Figure 6). From this analysis, a K_i of 50 ± 4 μM was determined, which matches the K_i calculated from IC_{50} determinations described above (52 ± 4 μM).

L-IPO (**13**) binds in a manner similar to that of related DDAH substrates (38,59,60), and places its terminal methyl group in the same position as the substrate's leaving group (N^{ω}-CH_3), indicating potential hydrophobic interactions with Leu271 (Figure 5). The amidine's N^{ω} also appear to make a hydrogen bond or ionic interaction with the carboxylate side chain of Glu78. We introduced several site-directed mutations to examine these interactions and their contributions to inhibitor potency (Table 2). Typical buried salt bridges have stabilization energies of approximately 3-4 kcal/mol (61), but Glu78 is also bridged to Lys175, diminishing the expected contribution of this interaction to L-IPO binding. Accordingly, an E78A mutation of DDAH-1 weakens the binding of L-IPO (**13**) by 1.9 kcal/mol. Typical hydrophobic interactions contribute approximately 1 kcal/mol/CH_2 (61). In DDAH-1, an L271G mutation weakens the binding of L-IPO (**13**) by 1.0 kcal/mol. Therefore, both charged and hydrophobic aspects of the amidine group contribute to the affinity of L-IPO. Additionally, mutation at the apex of the substrate-binding flap (not depicted), L30A, weakens L-IPO (**13**) binding, suggesting that, like substrate, the inhibitor's affinity is partially dependent on flap closure (Table 2). Changes in the circular dicroism spectrum of DDAH-1 upon L-IPO binding are minimal (Y. Wang, W. Fast, unpublished observations), indicating that no large-scale changes in secondary structure occur upon ligand binding. It is notable that changes to the k_{cat} and K_M values of these mutant proteins appear to be quite substrate dependent (Table 2), likely consistent with the influence of several kinetic steps on K_M values.

Because the structural model suggests a covalent mode of inhibition, time-dependence and reversibility of inhibition were examined. The onset of inhibition by L-IPO (**13**) is rapid, with no apparent time-dependence and no covalent adducts that are detected via ESI-MS after 18 h incubations (MW_{calc} = 33, 311 Da; MW_{exptl} = 33, 303 Da). Dilution of inhibited enzyme into inhibitor-free mixtures rapidly restores activity. These observations suggest that L-IPO (**13**) is not an irreversible or metabolically activated inhibitor. The possibility of slow L-IPO (**13**) hydrolysis catalyzed by DDAH-1 was also considered because hydrolysis proceeds through a tetrahedral adduct, and because slow substrates can act as de facto inhibitors. This is the case with L-arginine (**1**), a slow substrate of DDAH-1 and structural homolog of L-IPO (**13**) (Table 1). Two likely metabolites of L-IPO (**13**) are L-ornithine (L-Orn) and N^5-(1-oxopropyl)-L-ornithine, neither of which would be detectable by the diacetylmonoxime derivatization assay (29) typically used to detect substituted urea products of the DDAH-catalyzed reaction. Therefore, after incubation of L-IPO (**13**) with DDAH-1, the N^{α} group of remaining L-IPO (**13**) and the primary amines of any resulting reaction products were derivatized by *o*-phthalaldehyde and separated by HPLC to detect turnover. No new peaks appeared in the chromatogram after an 18 h incubation and the peak area corresponding to L-IPO (**13**) did not significantly change (not shown), indicating that hydrolysis of L-IPO (**13**) is not catalyzed by DDAH-1 over this timescale.

Experimental attempts were made to detect covalent bond formation between L-IPO and Cys274 in solution by monitoring ^{13}C-NMR shifts of the amidino C^{ξ} carbon of the inhibitor (Unpublished experiments: S. Hu, Y. Wang, D. Hoffman, W. Fast). Similar experiments with a peptide aldehyde inhibitor of papain revealed a 125 ppm upfield shift upon tetrahedral adduct formation between the active-site cysteine and the aldehyde inhibitor (62). With DDAH-1, formation of a tetrahedral adduct (**21**) between Cys274 and the C^{ξ} carbon of L-IPO is expected

to similarly shift the resonance of C^{ξ} considerably upfield (> 100 ppm) from its resonance in the sp^2 hybridized free ligand (Figure 5). In contrast, a purely non-covalent complex (**20**), would be expected to display a much more modest shift (< 10 ppm) for the C^{ξ} carbon upon binding (For related examples see (63-65)). Starting from ^{13}C-labeled potassium cyanide (99 atom % ^{13}C), L-IPO was synthesized with the C^{ξ} position isotopically enriched in ^{13}C. However, at a variety of stoichiometries and pH values, the bound inhibitor could not be detected by 1-dimensional ^{13}C-NMR (125.7 MHz), most likely due to line broadening of the signal. Therefore, this technique could not be used to detect covalent bond formation in solution.

In sum, the inhibitor L-IPO (**13**) and the substrate N^{ω}-methyl-L-arginine (**2**) have similar chemical structures, their only difference stemming from substitution of a guanidino-nitrogen with a methylene. Accordingly, L-IPO (**13**) acts as a competitive, non-hydrolyzable substrate analog that binds at the active site of DDAH-1 in a manner similar to substrate, but places a stable C-C bond in place of the scissile C^{ξ}-N^{ω} bond. Structural studies strongly suggest that Cys274 attacks the C^{ξ} carbon resulting in a tetrahedral adduct. This covalent adduct is expected to be in rapid equilibrium with the parent compound and the unmodified enzyme, consistent with the observation that inhibition is rapidly reversible. A similar tetrahedral complex was found to develop during crystal soaking of a related enzyme, arginine deiminase (66,67). Analogous reversible covalent inhibition has been reported of other thiol-dependent enzymes by nitriles, cyanamides and aldehydes, which form reversible thioimidate, thioamidine and hemithioacetal bonds, respectively (68-70). Also, structural studies of other reversible tetrahedral adducts have been reported, such as carbinolamine formation between pyruvate and Lys133 of aldolase (71).

The L-IPO-complexed DDAH-1 structure also reveals a perturbation of the active site His173 side chain in one molecule of the asymmetric unit (Figure 7). This histidine plays an essential role as a general acid and general base in the catalytic mechanism of DDAH (60,72), so changes at this position are noteworthy. When the structure of apo DDAH-1 is compared with the L-citrulline, L-IPO (**13**) or L-257 (**16**) complexes (Figure 7) (38), considerable variation is observed both in the conformation of the ligand and the orientation of some protein residues, most notably in the loop that precedes the active site His173 (^{169}ADGLH^{173}). His173 is positioned closest to the active-site ligand in the L-citrulline-bound structure, but is rotated farther away in the apo-, L-257 (**16**), and L-IPO (**13**) complexes. The loop proceeding His173 is most ordered in the apo structure and is similar to that seen in the L-IPO complex. However, some rearrangement and disorder of the loop is present in the L-citrulline complex and it is further rearranged in the L-257 complex, allowing for a bent conformation of the bound inhibitor. Relative to L-citrulline and L-IPO, a slight shift of the carboxylate of L-257 is also seen with a corresponding movement of Arg145, although this appears to be the result of side-chain repositioning rather than loop motion. If the L-IPO complex resembles a tetrahedral intermediate and the L-citrulline complex resembles the product complex, it is tempting to suggest that the observed conformational states resemble species found along the reaction coordinate, unlike the non-productive L-257 complex. However, additional evidence is needed to support such claims. Nonetheless, flexibility in both the ligand and the protein structures are observed, and these are important considerations for future inhibitor design and virtual screening efforts.

Toward a targeted polypharmacology to control NO

Despite the prevailing “one drug, one target” approach, there is growing evidence that supports the efficacy of selectively targeting multiple receptors by a single chemotherapeutic agent (73). Some of the many terms that encompass this approach include network pharmacology (74), targeted polypharmacology (75), designed multiple ligands (76), dirty drugs and magic

shotguns (77). Targeted pharmacology is quite different than the promiscuous inhibition that occurs through aggregation processes (78) and different than non-selective inhibition that affects irrelevant targets. Rather, multiple targets are specifically selected for the design of a single ligand that exploits overlapping pharmacophores. The need to bind different targets could alternatively be addressed by using combinations of single-target drugs, but the differential metabolism of each agent may vary between patients and can lead to very complex pharmacokinetic and pharmacodynamic behaviors that are difficult to predict. Therefore, a single-agent targeted polypharmacology approach is an attractive strategy.

DDAH and NOS represent a compelling combination for developing dual-targeted inhibitors to control biological NO production. Based on a limited exploration of the chemical space shared by NOS and DDAH ligands, we investigated a series of alkyl-substituted amidines to illuminate the similarities and differences between nNOS and DDAH-1 pharmacophores. In short, nNOS is effectively inhibited by amidines with alkyl substituents 2-5 carbons in length (including the sp^2 hybridized amidino-carbon) (**12**, **13**, **14**) (54), but potent DDAH-1 inhibition requires alkyl-substituents 3-6 carbons in length (**13**, **14**, **15**) (Figure 2). Therefore, by choosing the appropriate alkyl chain length, it is possible to selectively target either NOS or DDAH for inhibition, or to achieve dual inhibition of both enzymes. Comparison of inhibitor-bound structures of both DDAH and NOS reveals some of the active-site constraints that underlie this behavior (Figure 8). The active site of DDAH-1 is slightly larger and demonstrates structural plasticity of both protein residues and bound inhibitor, thereby allowing longer substituents. In contrast, the smaller active site of NOS limits the size of ligand by steric demands. Some plasticity in the NOS active site has been observed, but appears to be mediated by residues distant from the binding site of L-NIO (**12**) and its homologs (17). Therefore, the medium-length members of the alkyl-amidine series investigated here are able to occupy the common part of these overlapping pharmacophores, and a simple lengthening or shortening of the alkyl substituent can tip the specificity for one enzyme or the other. Although the bioavailabilities of most of these compounds have not been reported, we note that in activated macrophages, N^{ω}-methyl-L-arginine (**2**) and L-NIO (**12**) are effectively transported by the same y^+ cationic amino acid transporter as L-arginine (**1**) (79). These results should enable a more informed choice among pharmacological inhibitors of NO production, and will facilitate the future design of therapeutics and polypharmacological reagents to specifically impact NO production.

Acknowledgments

We thank Alexander Taylor for assistance with data collection at the X-ray Crystallography Core Laboratory at the University of Texas Health Science Center at San Antonio. We also thank David Hoffman (University of Texas, Austin) for assistance with ^{13}C NMR studies.

References

1. Hong L, Fast W. Inhibition of human dimethylargininase-1 (DDAH-1) by S-nitroso-L-homocysteine and hydrogen peroxide: analysis, quantification, and implications for hyperhomocysteinemia. J Biol Chem 2007;282:34684–34692. [PubMed: 17895252]
2. Ohshima H, Tatemichi M, Sawa T. Chemical basis of inflammation-induced carcinogenesis. Arch Biochem Biophys 2003;417:3–11. [PubMed: 12921773]
3. Xu W, Liu LZ, Loizidou M, Ahmed M, Charles IG. The role of nitric oxide in cancer. Cell Res 2002;12:311–20. [PubMed: 12528889]
4. Wink DA, Mitchell JB. Nitric oxide and cancer: an introduction. Free Radic Biol Med 2003;34:951–4. [PubMed: 12684080]
5. Jenkins DC, Charles IG, Thomsen LL, Moss DW, Holmes LS, Baylis SA, Rhodes P, Westmore K, Emson PC, Moncada S. Roles of nitric oxide in tumor growth. Proc Natl Acad Sci U S A 1995;92:4392–6. [PubMed: 7538668]

6. Thomsen LL, Miles DW. Role of nitric oxide in tumour progression: lessons from human tumours. Cancer Metastasis Rev 1998;17:107–18. [PubMed: 9544426]
7. Fukumura D, Kashiwagi S, Jain RK. The role of nitric oxide in tumour progression. Nat Rev Cancer 2006;6:521–34. [PubMed: 16794635]
8. Vallance P, Leiper J. Blocking NO synthesis: how, where and why? Nat Rev Drug Discov 2002;1:939–50. [PubMed: 12461516]
9. Tran CT, Leiper JM, Vallance P. The DDAH/ADMA/NOS pathway. Atheroscler Suppl 2003;4:33–40. [PubMed: 14664901]
10. Leiper J, Vallance P. Biological significance of endogenous methylarginines that inhibit nitric oxide synthases. Cardiovasc Res 1999;43:542–8. [PubMed: 10690326]
11. MacAllister RJ, Parry H, Kimoto M, Ogawa T, Russell RJ, Hodson H, Whitley GS, Vallance P. Regulation of nitric oxide synthesis by dimethylarginine dimethylaminohydrolase. Br J Pharmacol 1996;119:1533–40. [PubMed: 8982498]
12. Cardounel AJ, Zweier JL. Endogenous methylarginines regulate neuronal nitric-oxide synthase and prevent excitotoxic injury. J Biol Chem 2002;277:33995–4002. [PubMed: 12091378]
13. Ogawa T, Kimoto M, Sasaoka K. Purification and properties of a new enzyme, NG,NG-dimethylarginine dimethylaminohydrolase, from rat kidney. J Biol Chem 1989;264:10205–9. [PubMed: 2722865]
14. Dayoub H, Achan V, Adimoolam S, Jacobi J, Stuehlinger MC, Wang BY, Tsao PS, Kimoto M, Vallance P, Patterson AJ, Cooke JP. Dimethylarginine dimethylaminohydrolase regulates nitric oxide synthesis: genetic and physiological evidence. Circulation 2003;108:3042–7. [PubMed: 14638548]
15. Kostourou V, Robinson SP, Cartwright JE, Whitley GS. Dimethylarginine dimethylaminohydrolase I enhances tumour growth and angiogenesis. Br J Cancer 2002;87:673–80. [PubMed: 12237779]
16. Kostourou V, Robinson SP, Whitley GS, Griffiths JR. Effects of overexpression of dimethylarginine dimethylaminohydrolase on tumor angiogenesis assessed by susceptibility magnetic resonance imaging. Cancer Res 2003;63:4960–6. [PubMed: 12941821]
17. Garcin ED, Arvai AS, Rosenfeld RJ, Kroeger MD, Crane BR, Andersson G, Andrews G, Hamley PJ, Mallinder PR, Nicholls DJ, St-Gallay SA, Tinker AC, Gensmantel NP, Mete A, Cheshire DR, Connolly S, Stuehr DJ, Aberg A, Wallace AV, Tainer JA, Getzoff ED. Anchored plasticity opens doors for selective inhibitor design in nitric oxide synthase. Nat Chem Biol 2008;4:700–7. [PubMed: 18849972]
18. Silverman RB. Design of Selective Neuronal Nitric Oxide Synthase Inhibitors for the Prevention and Treatment of Neurodegenerative Diseases. Acc Chem Res. 2009
19. Ji H, Li H, Martasek P, Roman LJ, Poulos TL, Silverman RB. Discovery of Highly Potent and Selective Inhibitors of Neuronal Nitric Oxide Synthase by Fragment Hopping. J Med Chem. 2009
20. Pettersen EF, Goddard TD, Huang CC, Couch GS, Greenblatt DM, Meng EC, Ferrin TE. UCSF Chimera--a visualization system for exploratory research and analysis. J Comput Chem 2004;25:1605–12. [PubMed: 15264254]
21. Fast W, Nikolic D, VanBreemen RB, Silverman RB. Mechanistic Studies of the Inactivation of Inducible Nitric Oxide Synthase by N5(1-Iminoethyl)-L-ornithine (L-NIO). J Am Chem Soc 1999;121:903–916.
22. Moore WM, Webber RK, Jerome GM, Tjoeng FS, Misko TP, Currie MG. L-N6-(1-iminoethyl)lysine: a selective inhibitor of inducible nitric oxide synthase. J Med Chem 1994;37:3886–8. [PubMed: 7525961]
23. Bretscher LE, Li H, Poulos TL, Griffith OW. Structural characterization and kinetics of nitric-oxide synthase inhibition by novel N5-(iminoalkyl)- and N5-(iminoalkenyl)-ornithines. J Biol Chem 2003;278:46789–97. [PubMed: 12960153]
24. Babu BR, Griffith OW. N5-(1-Imino-3-butenyl)-L-ornithine. A neuronal isoform selective mechanism-based inactivator of nitric oxide synthase. J Biol Chem 1998;273:8882–9. [PubMed: 9535869]
25. Hong L, Fast W. Inhibition of human dimethylarginine dimethylaminohydrolase-1 by S-nitroso-L-homocysteine and hydrogen peroxide. Analysis, quantification, and implications for hyperhomocysteinemia. J Biol Chem 2007;282:34684–92. [PubMed: 17895252]

26. Stone EM, Person MD, Costello NJ, Fast W. Characterization of a transient covalent adduct formed during dimethylarginine dimethylaminohydrolase catalysis. Biochemistry 2005;44:7069–78. [PubMed: 15865451]
27. Geoghegan KF, Dixon HB, Rosner PJ, Hoth LR, Lanzetti AJ, Borzilleri KA, Marr ES, Pezzullo LH, Martin LB, LeMotte PK, McColl AS, Kamath AV, Stroh JG. Spontaneous alpha-N-6-phosphogluconoylation of a “His tag” in Escherichia coli: the cause of extra mass of 258 or 178 Da in fusion proteins. Anal Biochem 1999;267:169–84. [PubMed: 9918669]
28. Gill SC, von Hippel PH. Calculation of protein extinction coefficients from amino acid sequence data. Anal Biochem 1989;182:319–26. [PubMed: 2610349]
29. Knipp M, Vasak M. A colorimetric 96-well microtiter plate assay for the determination of enzymatically formed citrulline. Anal Biochem 2000;286:257–64. [PubMed: 11067748]
30. Stone EM, Fast W. A continuous spectrophotometric assay for dimethylarginine dimethylaminohydrolase. Anal Biochem 2005;343:335–7. [PubMed: 15992759]
31. Copeland, RA. Evaluation of enzyme inhibitors in drug discovery : a guide for medicinal chemists and pharmacologists. Wiley-Interscience; Hoboken, N.J.: 2005.
32. Cheng Y, Prusoff WH. Relationship between the inhibition constant (K1) and the concentration of inhibitor which causes 50 per cent inhibition (I50) of an enzymatic reaction. Biochem Pharmacol 1973;22:3099–108. [PubMed: 4202581]
33. Plevin MJ, Magalhaes BS, Harris R, Sankar A, Perkins SJ, Driscoll PC. Characterization and manipulation of the Pseudomonas aeruginosa dimethylarginine dimethylaminohydrolase monomer--dimer equilibrium. J Mol Biol 2004;341:171–84. [PubMed: 15312771]
34. Demeler, B. The University of Texas Health Science Center; San Antonio: 2005. www.ultrascan.uthscsa.edu
35. Otwinowski Z, Minor W. Processing of X-ray diffraction data collected in oscillation mode. Method Enzymol 1997;27:307–326.
36. Vagin A, Teplyakov A. MOLREP: an automated program for molecular replacement. J Appl Cryst 1997;30:1022–1025.
37. Kissinger CR, Gehlhaar DK, Smith BA, Bouzida D. Molecular replacement by evolutionary search. Acta Crystallogr D Biol Crystallogr 2001;57:1474–9. [PubMed: 11567162]
38. Leiper J, Nandi M, Torondel B, Murray-Rust J, Malaki M, O'Hara B, Rossiter S, Anthony S, Madhani M, Selwood D, Smith C, Wojciak-Stothard B, Rudiger A, Stidwill R, McDonald NQ, Vallance P. Disruption of methylarginine metabolism impairs vascular homeostasis. Nat Med 2007;13:198–203. [PubMed: 17273169]
39. McCoy AJ, Grosse-Kunstleve RW, Adams PD, Winn MD, Storoni LC, Read RJ. Phaser crystallographic software. J Appl Crystallogr 2007;40:658–674. [PubMed: 19461840]
40. Jones TA, Zou JY, Cowan SW, K M. Improved methods for building protein models in electron density maps and the locatin of errors in these models. Acta Cryst A 1991;47(Pt 2)
41. Brunger AT, Adams PD, Clore GM, DeLano WL, Gros P, Grosse-Kunstleve RW, Jiang JS, Kuszewski J, Nilges M, Pannu NS, Read RJ, Rice LM, Simonson T, Warren GL. Crystallography and NMR system: A new software suite for macromolecular structure determination. Acta Cryst D Biol Crystallogr 1998;54(Pt 5):905–921. [PubMed: 9757107]
42. Adams PD, Grosse-Kunstleve RW, Hung LW, Ioerger TR, McCoy AJ, Moriarty NW, Read RJ, Sacchettini JC, Sauter NK, Terwilliger TC. PHENIX: building new software for automated crystallographic structure determination. Acta Crystallogr D Biol Crystallogr 2002;58:1948–54. [PubMed: 12393927]
43. Read RJ. Improved Fourier coefficients for maps using phases from partial structures with errors. Acta Cryst Sect A 1986;42:140–149.
44. Brunger AT. Assessmet of phase accuracy by cross validation: the free R value. Methods and applications. Acta Cryst D Biol Crystallogr 1993;49:24–36. [PubMed: 15299543]
45. Laskowski RA, MacArthur MW, Moss DS, Thornton JM. PROCHECK: a program to check the stereochemical quality of protein structures. J Appl Cryst 1993;26:283–291.
46. Davis IW, Leaver-Fay A, Chen VB, Block JN, Kapral GJ, Wang X, Murray LW, Arendall WB 3rd, Snoeyink J, Richardson JS, Richardson DC. MolProbity: all-atom contacts and structure validation for proteins and nucleic acids. Nucleic Acids Res 2007;35:W375–83. [PubMed: 17452350]

47. Leiper JM, Santa Maria J, Chubb A, MacAllister RJ, Charles IG, Whitley GS, Vallance P. Identification of two human dimethylarginine dimethylaminohydrolases with distinct tissue distributions and homology with microbial arginine deiminases. Biochem J 1999;343(Pt 1):209–14. [PubMed: 10493931]
48. Garvey EP, Oplinger JA, Tanoury GJ, Sherman PA, Fowler M, Marshall S, Harmon MF, Paith JE, Furfine ES. Potent and selective inhibition of human nitric oxide synthases. Inhibition by non-amino acid isothioureas. J Biol Chem 1994;269:26669–76. [PubMed: 7523409]
49. Shearer BG, Lee S, Oplinger JA, Frick LW, Garvey EP, Furfine ES. Substituted N-phenylisothioureas: potent inhibitors of human nitric oxide synthase with neuronal isoform selectivity. J Med Chem 1997;40:1901–5. [PubMed: 9191968]
50. Narayanan K, Spack L, McMillan K, Kilbourn RG, Hayward MA, Masters BS, Griffith OW. S-alkyl-L-thiocitrullines. Potent stereoselective inhibitors of nitric oxide synthase with strong pressor activity in vivo. J Biol Chem 1995;270:11103–10. [PubMed: 7538112]
51. Jianmongkol S, Vuletich JL, Bender AT, Demady DR, Osawa Y. Aminoguanidine-mediated inactivation and alteration of neuronal nitric-oxide synthase. J Biol Chem 2000;275:13370–6. [PubMed: 10788446]
52. Wolff DJ, Gauld DS, Neulander MJ, Southan G. Inactivation of nitric oxide synthase by substituted aminoguanidines and aminoisothioureas. J Pharmacol Exp Ther 1997;283:265–73. [PubMed: 9336332]
53. Garvey EP, Oplinger JA, Furfine ES, Kiff RJ, Laszlo F, Whittle BJ, Knowles RG. 1400W is a slow, tight binding, and highly selective inhibitor of inducible nitric-oxide synthase in vitro and in vivo. J Biol Chem 1997;272:4959–63. [PubMed: 9030556]
54. Babu BR, Frey C, Griffith OW. L-arginine binding to nitric-oxide synthase. The role of H-bonds to the nonreactive guanidinium nitrogens. J Biol Chem 1999;274:25218–26. [PubMed: 10464242]
55. Rossiter S, Smith CL, Malaki M, Nandi M, Gill H, Leiper JM, Vallance P, Selwood DL. Selective substrate-based inhibitors of mammalian dimethylarginine dimethylaminohydrolase. J Med Chem 2005;48:4670–8. [PubMed: 16000003]
56. Kotthaus J, Schade D, Muschick N, Beitz E, Clement B. Structure-activity relationship of novel and known inhibitors of human dimethylarginine dimethylaminohydrolase-1: alkenyl-amidines as new leads. Bioorg Med Chem 2008;16:10205–9. [PubMed: 19013076]
57. Bogumil R, Knipp M, Fundel SM, Vasak M. Characterization of dimethylargininase from bovine brain: evidence for a zinc binding site. Biochemistry 1998;37:4791–8. [PubMed: 9537995]
58. Weickmann JL, Himmel ME, Smith DW, Fahrney DE. Arginine deiminase: demonstration of two active sites and possible half-of-the-sites reactivity. Biochem Biophys Res Commun 1978;83:107–13. [PubMed: 697802]
59. Murray-Rust J, Leiper J, McAlister M, Phelan J, Tilley S, Santa Maria J, Vallance P, McDonald N. Structural insights into the hydrolysis of cellular nitric oxide synthase inhibitors by dimethylarginine dimethylaminohydrolase. Nat Struct Biol 2001;8:679–83. [PubMed: 11473257]
60. Linsky TW, Monzingo AF, Stone EM, Robertus JD, Fast W. Promiscuous partitioning of a covalent intermediate common in the pentein superfamily. Chem Biol 2008;15:467–75. [PubMed: 18482699]
61. Petsko, GA.; Ringe, D. Protein structure and function. New Science Press; Sinauer Associates Blackwell Pub.; London Sunderland, MA Oxford: 2004.
62. Gamcsik MP, Malthouse JPG, Primrose WU, Mackenzie NE, Boyd ASF, Russell RA, Scott AI. Structure and Stereochemistry of Tetrahedral Inhibitor Complexes of Papain by Direct NMR Observation. J Am Chem Soc 1983;105:6324–6325.
63. Mackenzie NE, Malthouse JP, Scott AI. Studying enzyme mechanism by 13C nuclear magnetic resonance. Science 1984;225:883–9. [PubMed: 6433481]
64. Malthouse JP, Mackenzie NE, Boyd ASF, Scott AI. Detection of a tetrahedral adduct in a trypsin-chloromethyl ketone specific inhibitor complex by 13C NMR. J Am Chem Soc 1983;105:1685–1686.
65. Richarz R, Tschesche H, Wuthrich K. Carbon-13 nuclear magnetic resonance studies of the selectively isotope-labeled reactive site peptide bond of the basic pancreatic trypsin inhibitor in the complexes with trypsin, trypsinogen, and anhydrotrypsin. Biochemistry 1980;19:5711–5. [PubMed: 6161642]

66. Galkin A, Lu X, Dunaway-Mariano D, Herzberg O. Crystal structures representing the Michaelis complex and the thiouronium reaction intermediate of Pseudomonas aeruginosa arginine deiminase. J Biol Chem 2005;280:34080–7. [PubMed: 16091358]

67. Das K, Butler GH, Kwiatkowski V, Clark AD Jr, Yadav P, Arnold E. Crystal structures of arginine deiminase with covalent reaction intermediates; implications for catalytic mechanism. Structure (Camb) 2004;12:657–67. [PubMed: 15062088]

68. Falgueyret JP, Oballa RM, Okamoto O, Wesolowski G, Aubin Y, Rydzewski RM, Prasit P, Riendeau D, Rodan SB, Percival MD. Novel, nonpeptidic cyanamides as potent and reversible inhibitors of human cathepsins K and L. J Med Chem 2001;44:94–104. [PubMed: 11141092]

69. Mackenzie NE, Grant SK, Scott AI, Malthouse JP. 13C NMR study of the stereospecificity of the thiohemiacetals formed on inhibition of papain by specific enantiomeric aldehydes. Biochemistry 1986;25:2293–8. [PubMed: 3707946]

70. Liang TC, Abeles RH. Inhibition of papain by nitriles: mechanistic studies using NMR and kinetic measurements. Arch Biochem Biophys 1987;252:626–34. [PubMed: 3813553]

71. Allard J, Grochulski P, Sygusch J. Covalent intermediate trapped in 2-keto-3-deoxy-6-phosphogluconate (KDPG) aldolase structure at 1.95-A resolution. Proc Natl Acad Sci U S A 2001;98:3679–84. [PubMed: 11274385]

72. Stone EM, Costello AL, Tierney DL, Fast W. Substrate-assisted cysteine deprotonation in the mechanism of dimethylargininase (DDAH) from Pseudomonas aeruginosa. Biochemistry 2006;45:5618–30. [PubMed: 16634643]

73. Hopkins AL, Mason JS, Overington JP. Can we rationally design promiscuous drugs? Curr Opin Struct Biol 2006;16:127–36. [PubMed: 16442279]

74. Hopkins AL. Network pharmacology: the next paradigm in drug discovery. Nat Chem Biol 2008;4:682–90. [PubMed: 18936753]

75. Apsel B, Blair JA, Gonzalez B, Nazif TM, Feldman ME, Aizenstein B, Hoffman R, Williams RL, Shokat KM, Knight ZA. Targeted polypharmacology: discovery of dual inhibitors of tyrosine and phosphoinositide kinases. Nat Chem Biol 2008;4:691–9. [PubMed: 18849971]

76. Morphy R, Rankovic Z. Designed multiple ligands. An emerging drug discovery paradigm. J Med Chem 2005;48:6523–43. [PubMed: 16220969]

77. Roth BL, Sheffler DJ, Kroeze WK. Magic shotguns versus magic bullets: selectively non-selective drugs for mood disorders and schizophrenia. Nat Rev Drug Discov 2004;3:353–9. [PubMed: 15060530]

78. Coan KE, Shoichet BK. Stoichiometry and physical chemistry of promiscuous aggregate-based inhibitors. J Am Chem Soc 2008;130:9606–12. [PubMed: 18588298]

79. Baydoun AR, Mann GE. Selective targeting of nitric oxide synthase inhibitors to system y+ in activated macrophages. Biochem Biophys Res Commun 1994;200:726–31. [PubMed: 7513994]

80. Reif DW, McCreedy SA. N-nitro-L-arginine and N-monomethyl-L-arginine exhibit a different pattern of inactivation toward the three nitric oxide synthases. Arch Biochem Biophys 1995;320:170–6. [PubMed: 7540822]

81. Rogers NE, Ignarro LJ. Constitutive nitric oxide synthase from cerebellum is reversibly inhibited by nitric oxide formed from L-arginine. Biochem Biophys Res Commun 1992;189:242–9. [PubMed: 1280418]

82. Li H, Raman CS, Martasek P, Masters BS, Poulos TL. Crystallographic studies on endothelial nitric oxide synthase complexed with nitric oxide and mechanism-based inhibitors. Biochemistry 2001;40:5399–406. [PubMed: 11331003]

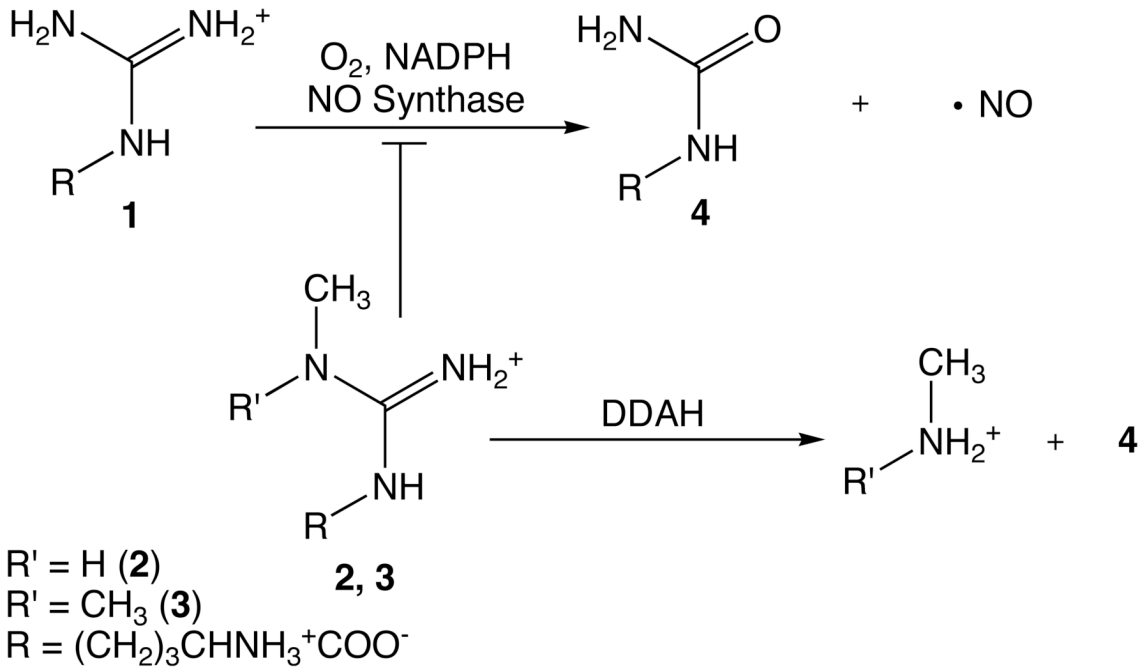

Figure 1.
Nitric oxide biosynthesis is promoted by the enzymic activities of both NO synthase (NOS) and DDAH. DDAH catabolizes endogenous methylarginines and relieves their inhibition of NOS.

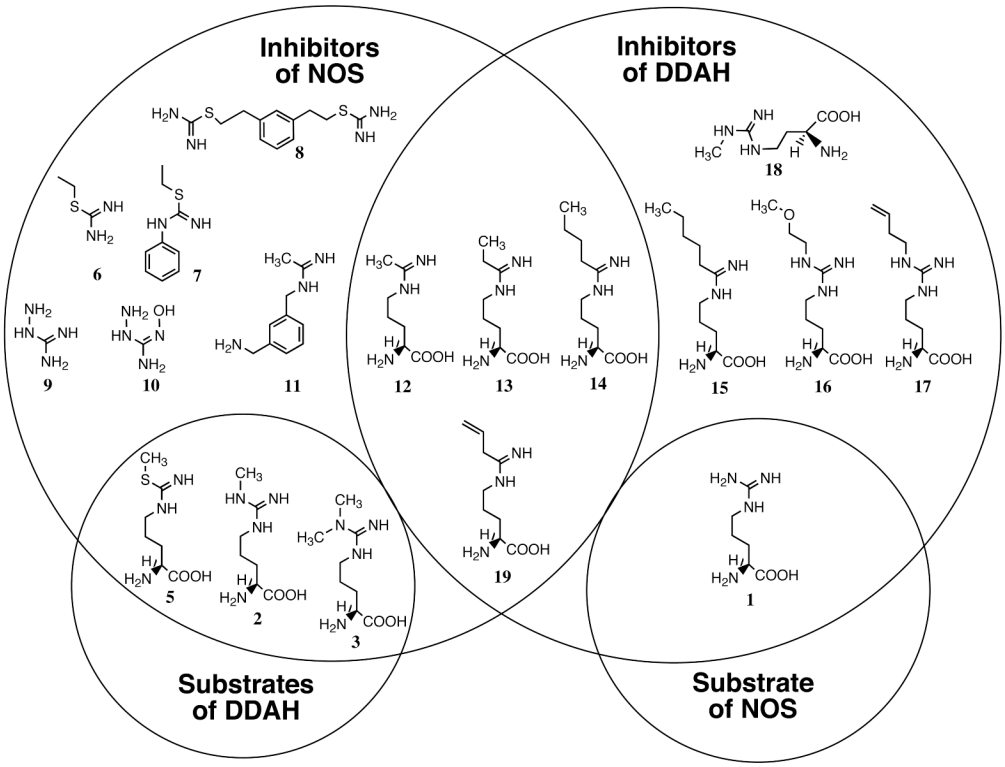

Figure 2.
Diagram of selected substrates and inhibitors of NOS and DDAH-1.

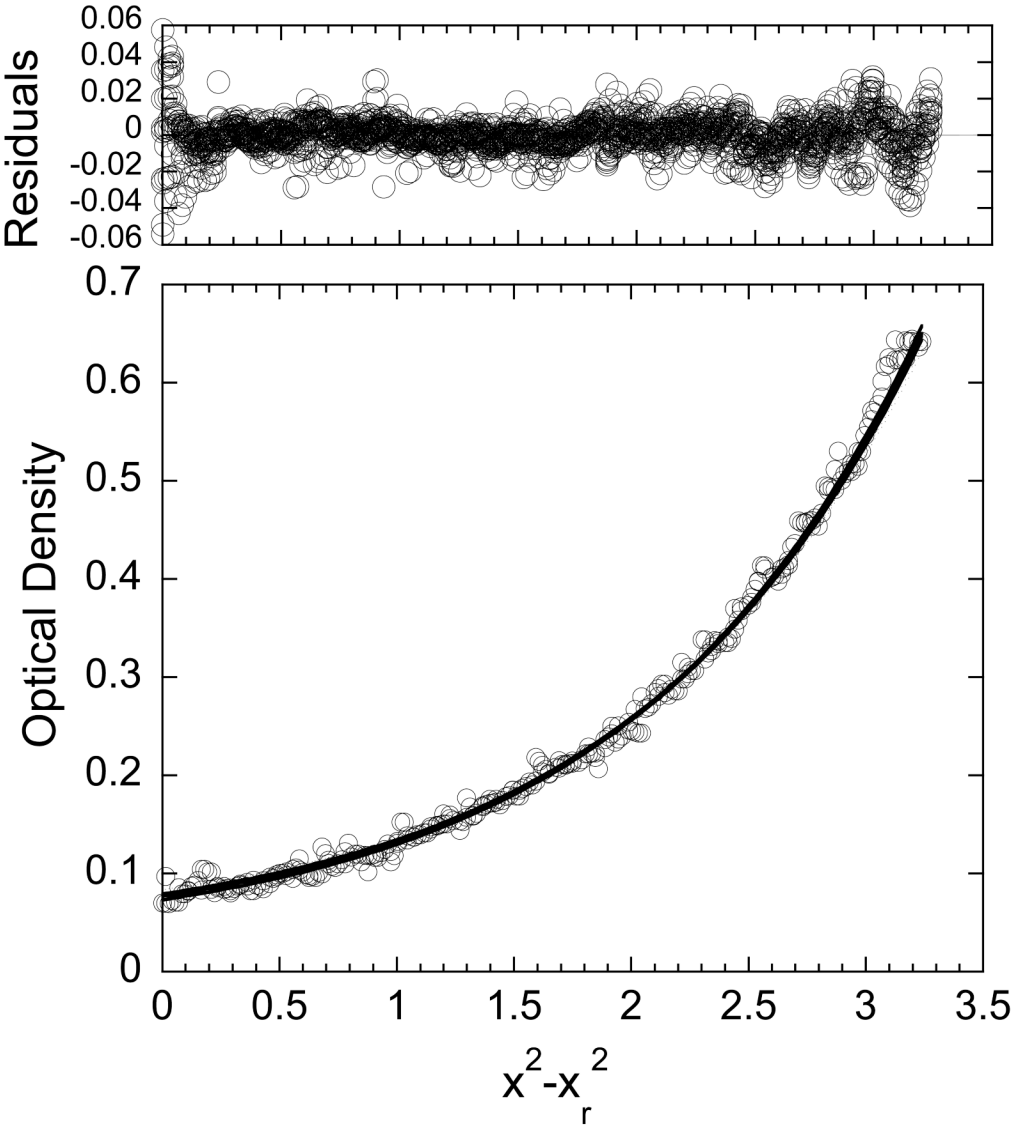

Figure 3.

Analytical sedimentation equilibrium ultracentrifugation of DDAH-1. Symbols represent an overlay of data collected during the last nine scans, indicative that equilibrium had been reached. The solid line represents the global simultaneous fit for a single ideal species model using Ultrascan. The fitted M_w is 34,530 Da (theoretical monomer M_w = 33,558 Da), variance = $8.7e^{-5}$. Conditions: DDAH-1 (1 mg/ mL), NaH_2PO_4 (20 mM), NaCl (100 mM), pH 7.0 at 25 °C with a rotor speed of 20,000 rpm.

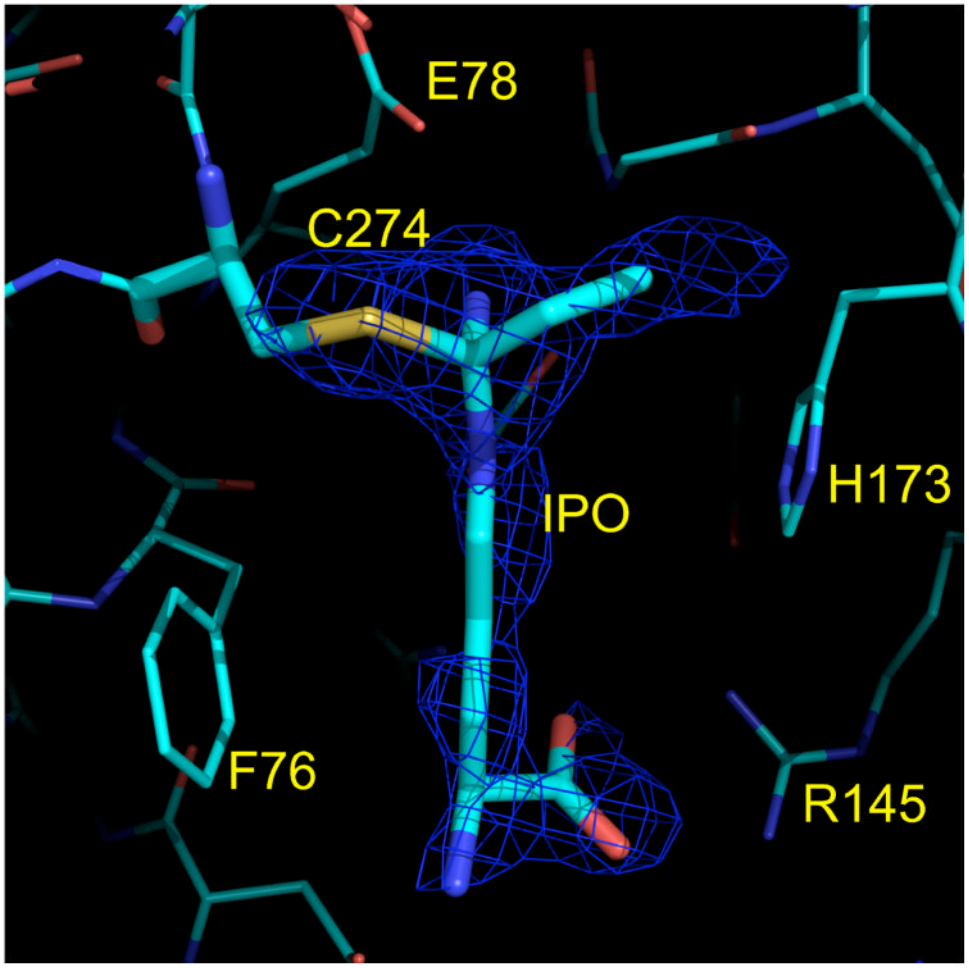

Figure 4.

The active site of DDAH-1 in complex with L-IPO (**13**) and omit map density. Atoms colored in cyan, blue, red and yellow for carbon, nitrogen, oxygen and sulfur, respectively. Active-site residues and L-IPO are labeled. The F_o-F_c electron density map, with L-IPO and the C274 Sγ atom not included in the calculated structure factors, is shown at 3 σ in blue.

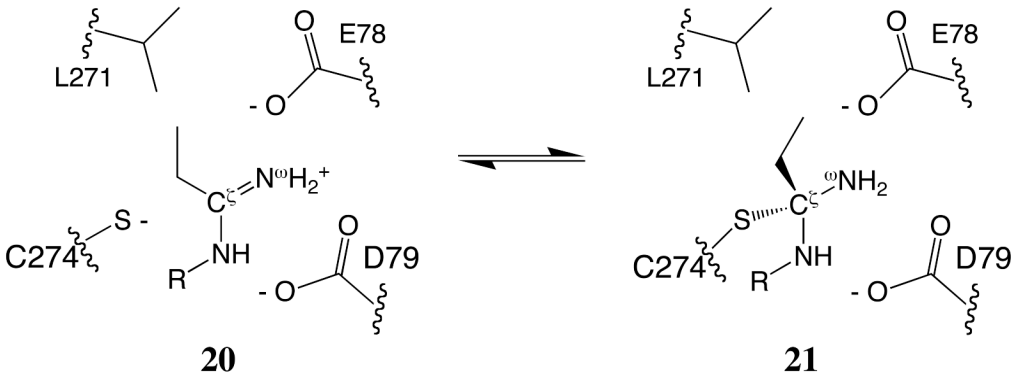

Figure 5.

Reversible covalent inhibition of DDAH-1 by L-IPO (**13**). The the non-covalent complex (**20**) is expected to be in rapid equilibrium with the (*R*)-tetrahedral complex (**21**).

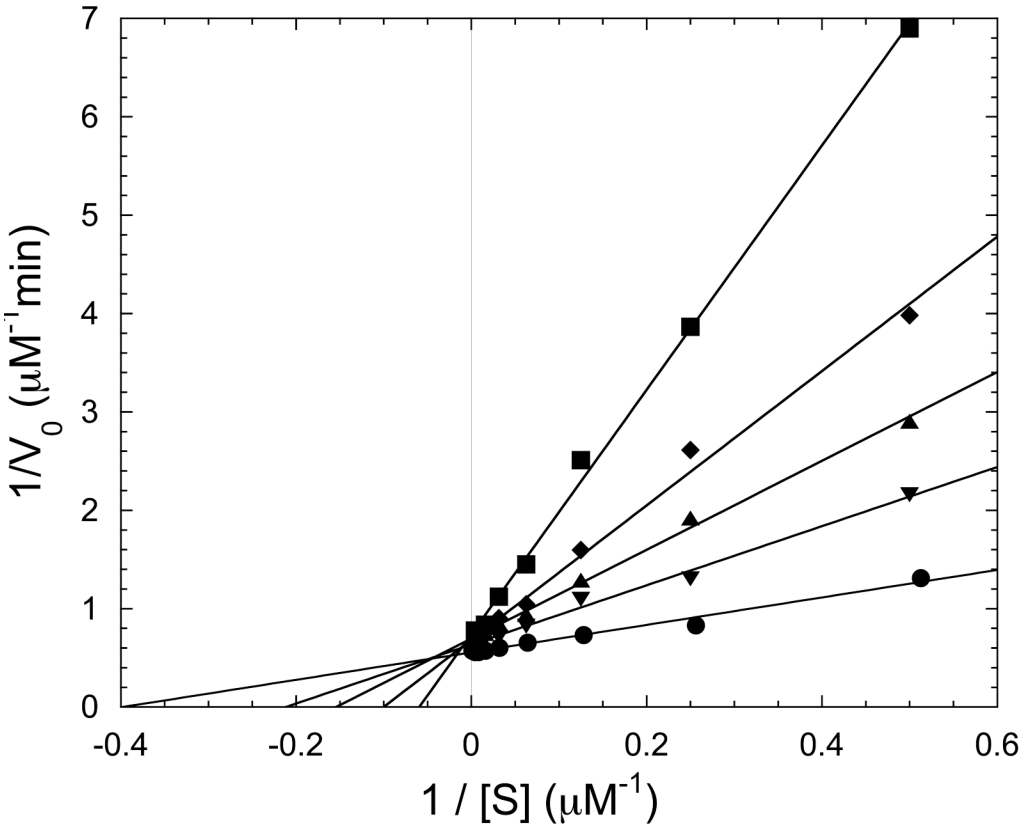

Figure 6.

Lineweaver-Burk plot of DDAH-1 inhibition by L-IPO (13). L-IPO is included in assay mixtures at 0 (●), 62.5 (▼), 125 (▲), 250 (□) and 500 (■) μM at pH 7.27, 25 °C. Intersecting fits at $1/V_{max}$ indicates competitive inhibition against the SMTC substrate. A K_i value of 50 ± 4 μM is determined as described in Experimental Procedures.

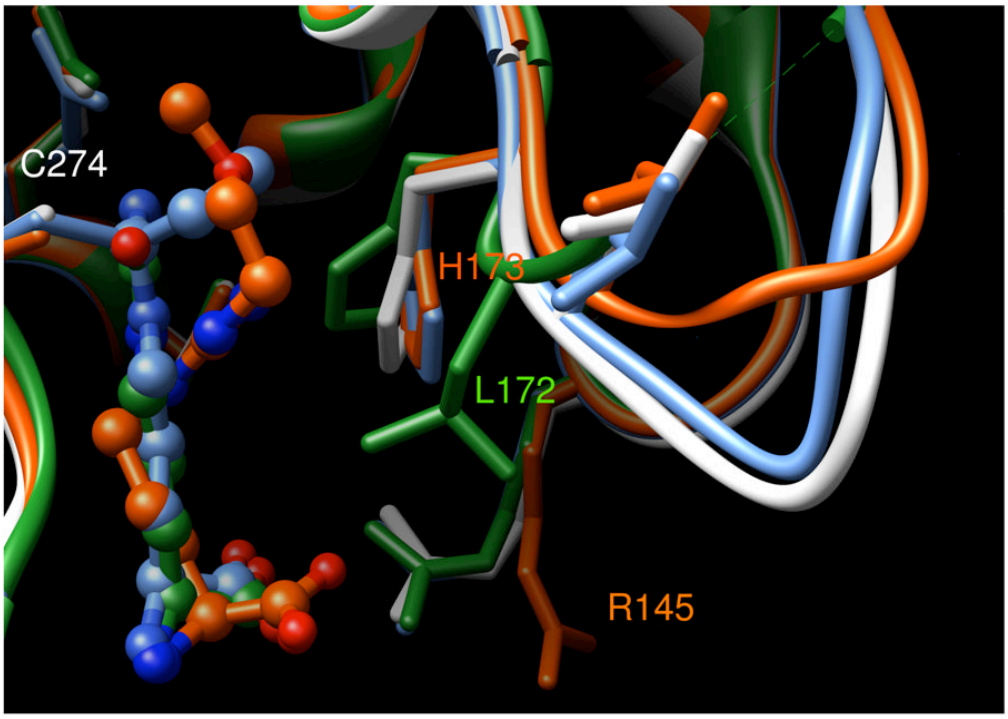

Figure 7.
Alternative loop conformations observed in DDAH-1. Structural variance in residues 167 – 173 is observed depending on the bound inhibitor. Protein backbone is shown as a ribbon representation, bound inhibitors as ball and stick representations, and selected residues (Arg 145, Leu172, His 173, Cys 274) in stick form. Apo protein is in white, and the L-citrulline (**4**), L-IPO (**13**) and L-257 (**16**) complexed structures in green, light blue and orange, respectively. The figure is constructed using coordinates from this work and from protein data bank accession codes 2JAI and 2JAJ (38).

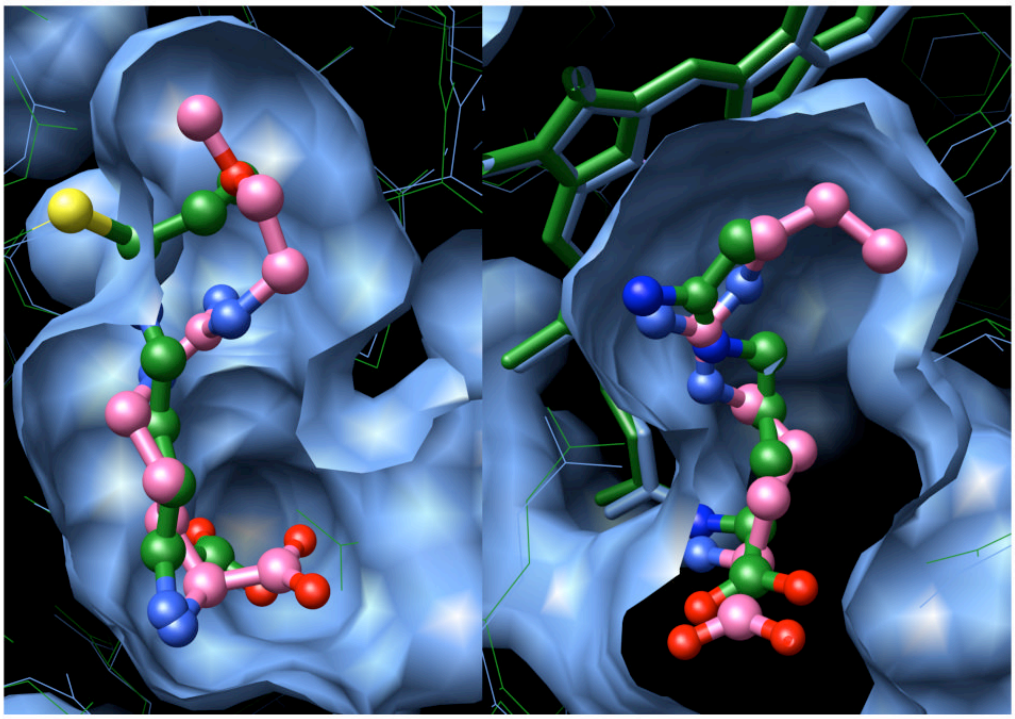

Figure 8.

Comparison of DDAH-1 and NOS active sites. The left panel shows a superimposition of human DDAH-1 with bound L-IPO (**13**) (green) and L-257 (**16**) (pink). The right panel shows a superimposition of bovine eNOS bound by L-NIO (**12**) (green) and rat nNOS bound by N^{ω}-propyl-L-arginine (pink), a compound of comparable length to N^{5}-(1-iminopentyl)-L-ornithine (**14**). Inhibitors are shown in ball and stick format and colored by heteroatom as described earlier. The heme groups of NOS are shown in stick models. Surface features (light blue) are shown for the L-257-DDAH-1 complex and the N^{ω}-propyl-L-arginine-nNOS complex to highlight the active-site cavity shape. Figures are constructed using coordinates from this work and protein data bank accession codes 2JAJ, 1ED6 and 1MMV (23,38,82).

Table 1

Substrates and Inhibitors of DDAH-1 and nNOS

Compound	DDAH-1		nNOS	
	K_i (μM)[a]	K_M (μM)	K_i (μM)	K_M (μM)
NMMA (**2**)	ND [b]	90 ± 10 [c]	2.0[d]	ND
ADMA (**3**)	ND	110 ± 14 [c]	0.7[e]	ND
SMTC (**5**)	ND	3.1 ± 0.3	0.05 ± 0.01[f]	ND
L-Arginine (**2**)	131 ± 7	ND	ND	1.6 ± 0.3[i]
L-Citrulline (**4**)	3,700 ± 200	ND	> 1 mM[g]	ND
L-NIO (**12**)	990 ± 80	ND	1.7[h]	ND
L-IPO (**13**)	52 ± 4	ND	3.0[h]	ND
L-IBO	59 ± 3	ND	ND	ND
(**14**)	7.5 ± 0.4	ND	20 ± 4[i]	ND
(**15**)	110 ± 10	ND	> 1,900[j]	ND

[a] calculated from IC_{50} values as described in Experimental Procedures

[b] Not Determined

[c] human DDAH-1 (1)

[d] K_I value for human nNOS (80)

[e] rat nNOS (12)

[f] rat nNOS (50)

[g] rat nNOS (81)

[h] rat nNOS (24)

[i] human nNOS (23)

[j] IC_{50} value for rat nNOS (54)

Table 2

Effects of mutations on steady-state kinetics and IPO binding

Enzyme	Substrate	K_{cat} (min^{-1})	K_M (μM)	*k*cat/*K*M (min^{-1} mM^{-1})	L-IPO (13) K_i[a] (μM)	ΔΔGbinding[b] (kcal/mol)
Wild-type	ADMA	0.86 ± 0.02	110 ± 14	8 ± 1		
	SMTC	2.51 ± 0.02	3.1 ± 0.3	810 ± 80	52 ± 4	NA[c]
L30A	ADMA	1.01 ± 0.06	1,400 ± 250	0.7 ± 0.2		
	SMTC	2.51 ± 0.02	3.6 ± 0.2	700 ± 40	1,400 ± 80	2.0
E78A	ADMA	0.09 ± 0.01	13,700 ± 2,700[d]	0.007 ± 0.002		
	SMTC	1.8 ± 0.5	19 ± 3	95 ± 40	1,200 ± 100	1.9
L271G	ADMA	0.52 ± 0.01	750 ± 70	0.69 ± 0.08		
	SMTC	0.58 ± 0.01	1.4 ± 0.2	410 ± 70	290 ± 20	1.0

[a] K_i values calculated from IC_{50} values determined using SMTC as a substrate (Materials and Methods)

[b] ΔΔGbinding= *RT*ln(*K*i, mutant/*K*i, wild-type)

[c] Not Applicable

[d] estimate. Highest [ADMA] tested was 10 mM.

Table 3

Crystallographic Data

	Apo-DDAH-1	L-IPO complex
PDB code	3I2E	3I4A
Space group	$P2_1$	$P2_1$
Cell constants	a=73.0, b=47.9, c=90.3 Å, β=94.1°	a=47.6, b=80.1, c=73.9 Å, β=90.1°
Resolution (Å)	20.-2.0 (2.1-2.0)[a]	20.-1.9 (1.93-1.90)
R_{merge} (%)	0.074 (0.225)	0.065 (0.39)
$<I/\sigma_I>$	9.5 (6.0)	10.5 (2.5)
Completeness (%)	99.9 (99.8)	96.1 (94.7)
Unique reflections	40,755	42,222
Redundancy	4.4	3.7
# of molecules per asymmetric unit	2	2
# of residues	550	550
# of protein atoms	4195	4108
# of ligand atoms	NA[b]	26
# of solvent atoms	528	99
$R_{working}$	0.189	0.174
R_{free}	0.225	0.244
Average B factor for protein atoms ($Å^2$)	16.9	30.5
Average B factor for ligand atoms ($Å^2$)	NA	24.8
Average B factor for solvent atoms ($Å^2$)	24.2	28.1
rms deviation from ideality		
bonds (Å)	0.004	0.007
angles (°)	1.309	1.110
Ramachandran plot		
% of residues in most favored region	96.7	94.0
% of residues in additional allowed region	3.3	6.0

[a] Values in parentheses correspond to highest resolution shell

[b] Not applicable